Quantification of Human and Rodent Brown Adipose Tissue Function Using ^{99m}Tc-Methoxyisobutylisonitrile SPECT/CT and ^{18}F-FDG PET/CT

Aaron M. Cypess[1], Ashley N. Doyle[2], Christina A. Sass[1], Tian Lian Huang[1], Peter M. Mowschenson[3], Harold N. Rosen[4], Yu-Hua Tseng[1], Edwin L. Palmer III[5], and Gerald M. Kolodny[6]

[1]Section of Integrative Physiology and Metabolism, Research Division, Joslin Diabetes Center, Harvard Medical School, Boston, Massachusetts; [2]Harvard-Thorndike Clinical Research Center, Beth Israel Deaconess Medical Center, Harvard Medical School, Boston, Massachusetts; [3]Department of Surgery, Beth Israel Deaconess Medical Center, Harvard Medical School, Boston, Massachusetts; [4]Division of Endocrinology, Department of Medicine, Beth Israel Deaconess Medical Center, Harvard Medical School, Boston, Massachusetts; [5]Division of Nuclear Medicine, Department of Radiology, Massachusetts General Hospital, Harvard Medical School, Boston, Massachusetts; and [6]Division of Nuclear Medicine, Department of Radiology, Beth Israel Deaconess Medical Center, Harvard Medical School, Boston, Massachusetts

For brown adipose tissue (BAT) to be effective at consuming calories, its blood flow must increase enough to provide sufficient fuel to sustain energy expenditure and also transfer the heat created to avoid thermal injury. Here we used a combination of human and rodent models to assess changes in BAT blood flow and glucose utilization. **Methods**: ^{99m}Tc-methoxyisobutylisonitrile (MIBI) SPECT ($n = 7$) and SPECT/CT ($n = 74$) scans done in adult humans for parathyroid imaging were reviewed for uptake in regions consistent with human BAT. Site-directed biopsies of subcutaneous and deep neck fat were obtained for electron microscopy and gene expression profiling. In mice, tissue perfusion was measured with ^{99m}Tc-MIBI ($n = 16$) and glucose uptake with ^{18}F-FDG ($n = 16$). Animals were kept fasting overnight, anesthetized with pentobarbital, and given intraperitoneally either the β_3-adrenergic receptor agonist CL-316,243, 1 mg/kg ($n = 8$), or saline ($n = 8$) followed by radiotracer injection 5 min later. After 120 min, the mice were imaged using SPECT/CT or PET/CT. Vital signs were recorded over 30 min during the imaging. BAT, white adipose tissue (WAT), muscle, liver, and heart were resected, and tissue uptake of both ^{99m}Tc-MIBI and ^{18}F-FDG was quantified by percentage injected dose per gram of tissue and normalized to total body weight. **Results:** In 5.4% of patients (4/74), ^{99m}Tc-MIBI SPECT/CT showed increased retention in cervical and supraclavicular fat that displayed multilocular lipid droplets, dense capillary investment, and a high concentration of ovoid mitochondria. Expression levels of the tissue-specific uncoupling protein-1 were 180 times higher in BAT than in subcutaneous WAT ($P < 0.001$). In mice, BAT tissue perfusion increased by 61% ($P < 0.01$), with no significant changes in blood flow to WAT, muscle, heart, or liver. CL-316,243 increased glucose uptake in BAT even more, by 440% ($P < 0.01$). **Conclusion:** Pharmacologic activation of BAT requires increased blood flow to deliver glucose and oxygen for thermogenesis. However, the glucose consumption far exceeds the vascular response. These findings demonstrate that activated BAT increases glucose uptake beyond what might occur by increased blood flow alone and suggest that activated BAT likely uses glucose for nonthermogenic purposes.

Key Words: brown fat; blood flow; glucose uptake

J Nucl Med 2013; 54:1896–1901
DOI: 10.2967/jnumed.113.121012

The contemporary pandemics of obesity and diabetes are devastating in size, breadth, and rate of growth (*1*). Central to these pathologic processes is the adipose tissue depot. White adipose tissue (WAT) stores energy and in excess results in obesity and insulin resistance, whereas brown adipose tissue (BAT) consumes calories for the purpose of thermogenesis via tissue-specific uncoupling protein-1 (UCP1) (*2*). BAT was initially known for its role in nonshivering and diet-induced thermogenesis in infants and small mammals (*3*), but it has been recently shown that adult humans have detectable BAT (*4–10*). When activated by mild cold exposure, human BAT consumes more glucose per gram than any other tissue (*11*), suggesting that BAT activity may be used to treat metabolic dysfunction.

Although there is great therapeutic potential in the use of human BAT energy expenditure, little is known about the details underlying its physiologic response to stimulation. Currently, BAT is routinely imaged via ^{18}F-FDG PET/CT, which has been useful in epidemiologic (*12*) and functional (*13–16*) studies. This approach has its limitations since glucose retention may not reflect the actual energy expenditure of the tissue (*17*). PET studies using ^{15}O and ^{11}C have been helpful in demonstrating BAT perfusion (*11*) and aerobic respiration (*18*), respectively, but their short half-lives substantially reduce their utility. An attractive alternative is ^{99m}Tc-methoxyisobutylisonitrile (MIBI), a perfusion-mediated radiotracer that is readily accessible and can provide essential information about BAT blood flow in adult humans (*19,20*).

Received Feb. 1, 2013; revision accepted May 17, 2013.
For correspondence or reprints contact: Aaron M. Cypess, Section of Integrative Physiology and Metabolism, Research Division, Joslin Diabetes Center, One Joslin Place, Boston, MA, 02215.
E-mail: aaron.cypess@joslin.harvard.edu
Published online Sep. 26, 2013.

BAT activity in both humans and rodent models is routinely achieved through cold exposure (*6,8,21*), which acts centrally to stimulate the sympathetic nervous system to release norepinephrine from postganglionic neurons and activate UCP1 and thermogenesis in BAT (*22*). Observational studies support the possibility that ^{99m}Tc-MIBI could localize to human BAT (*23–26*). However, it is not yet known how BAT tissue perfusion responds to pharmacologic stimulation. In the current study, we provided the first (to our knowledge) direct physical evidence that ^{99m}Tc-MIBI localizes to adult human BAT in vivo. We then used a rodent model to evaluate uptake after stimulation with CL-316,243 (*27*), an agonist for the β_3-adrenergic receptor, which is highly expressed in adipose tissue. Using ^{99m}Tc-MIBI and ^{18}F-FDG, we established the relationship between the increase in tissue perfusion and glucose uptake after pharmacologic stimulation of mouse BAT.

MATERIALS AND METHODS

Patients

This study followed institutional guidelines and was approved by the ethics committees of Beth Israel Deaconess Medical Center, Partners HealthCare, and Joslin Diabetes Center, all in Boston, MA. For the medical records review and discarded material analyses, the consent of patients was not required. The Harvard Medical School Shared Pathology Informatics Network Patients database was used to identify patients at Massachusetts General Hospital who had undergone ^{99m}Tc-MIBI SPECT to locate parathyroid adenomas and also had tissue processed for clinical indications during subsequent parathyroidectomies that were officially documented by staff pathologists as having brown adipocytes. For the ^{99m}Tc-MIBI SPECT/CT dataset at Beth Israel Deaconess Medical Center, consecutive studies over a 22-mo period were assessed for the presence of activity in regions associated with brown fat. Written informed consent was obtained from the patient from whom the prospective biopsy was obtained.

Human Parathyroid Imaging with ^{99m}Tc-MIBI

For planar imaging, patients were injected intravenously with 740 MBq (20 mCi) of ^{99m}Tc-MIBI. Immediately and then 1.5 h after injection, 10-min anterior, 35° right anterior oblique, and 35° left anterior oblique planar images were acquired in a 128 × 128 matrix, with a 20% window centered around the 140-keV photopeak, using a low-energy, high-resolution parallel collimator in an e.cam nuclear γ camera (Siemens Medical Systems). For SPECT/CT, imaging was performed as described previously (*28*) and in the supplemental methods (supplemental materials are available at http://jnm.snmjournals.org). All patients were injected intravenously with 740 MBq (20 mCi) of ^{99m}Tc-MIBI, and planar dual-phase imaging was performed with standard parameters after 20 min and 2 h using a Precedence SPECT/CT scanner (Philips). CT Images were used for attenuation correction and anatomic localization. Static views were obtained 20 min after tracer injection, followed by SPECT/CT imaging after the 20-min static views, and finally 2-h planar views.

Processing of Human Tissue

^{99m}Tc-MIBI SPECT/CT scans were done for the clinical purpose of identifying parathyroid adenomas. Patients whose scans indicated the presence of BAT were selected. The precise anatomic location of the adipose tissue with increased uptake of ^{99m}Tc-MIBI was reviewed with the surgeon who then resected the fat tissue, providing site-directed biopsies of human neck subcutaneous white fat and deeper brown fat. The fat was prepared for light and electron microscopy as described previously (*29*).

Human Gene Expression

Human gene expression experiments were performed as described previously (*30*). BAT and WAT were collected and stored in liquid nitrogen at −80°C. RNA was extracted from tissue using QIAzol and RNEasy kits (QIAGEN). Complementary DNA was made using a High-Capacity cDNA Reverse Transcription Kit (Applied Biosystems), and quantitative real-time polymerase chain reaction was performed using complementary DNA with SybrGreen Master Mix (Fisher) (Supplemental Table 1). Polymerase chain reaction was run using the ABI Prism 7900 sequence detection system (Applied Biosystems). Expression levels of genes associated with BAT (*UCP1*, *DIO2*, *CideA*, *PGC1α*) and WAT (*leptin*) were normalized to 36B4.

Rodent Imaging Protocol

All animal studies were approved by the Institutional Animal Care and Usage Committees at Joslin Diabetes Center and Beth Israel Deaconess Medical Center. Full details of the imaging protocols are provided in the supplemental methods. In brief, after overnight fasting, 32 mice (129SVE, 8–16 wk old, 20–30 g; Taconic) were anesthetized with sodium pentobarbital (50–75 mg/kg intraperitoneally, followed by 20 mg/kg intraperitoneally every 30 min starting 1 h after the initial dose) and then given either the β_3-adrenergic receptor agonist CL-316,243, 1 mg/kg (n = 16), or saline (n = 16) followed 5–10 min later by either ^{18}F-FDG, 10.2 MBq (275 μCi) (n = 8 for each of the 2 treatments), or ^{99m}Tc-MIBI, 8.3 MBq (225 μCi) (n = 8 for each of the 2 treatments). Two hours later, the mice were imaged using PET/CT or SPECT/CT, respectively. Imaging was performed on a NanoSPECT/CT (Bioscan) and a NanoPET/CT (Mediso Medical Imaging Systems). Helical small-animal SPECT was performed using a 4-head γ camera outfitted with multipinhole collimators (1.0-mm-diameter pinholes) for a single mouse scan. Reconstruction was performed using Nucline software (Mediso Medical Imaging Systems) in 2-dimensional mode. Ordered-subsets expectation maximization reconstruction was used with a single-slice rebinning 2-dimensional line-of-response method. Respiratory rate was measured using a small-animal monitoring and gating system (model 1025T; SA Instruments), and heart rate was measured using a neonatal, prewired, radiolucent monitoring electrode with clear tape (Red Dot; 3M). Vital signs were recorded over 30 min during the imaging. At the end of the imaging session, the mice were sacrificed and interscapular BAT, posterior subcutaneous WAT, muscle, liver, and heart tissue were dissected and weighed. Tissue radioactivity for both ^{99m}Tc-MIBI and ^{18}F-FDG was measured using percentage injected dose per gram of tissue, normalized to total body weight (%ID/g × kg).

Statistical Analyses

Data were analyzed using JMP Pro 9.0.0 software (SAS Institute, Inc.). All P values presented are 2-tailed, and a P value of less than 0.05 was considered to indicate statistical significance. Comparison of the gene expression in different anatomic depots was done using the Student t test.

RESULTS

^{99m}Tc-MIBI Localizes to BAT in Adult Humans

To prove that ^{99m}Tc-MIBI was localizing to BAT, we first reviewed all SPECT scans done over a 3-y period in which biopsy tissue was available and showed the presence of brown adipocytes. Nine patients met these criteria. The delayed images showed in-

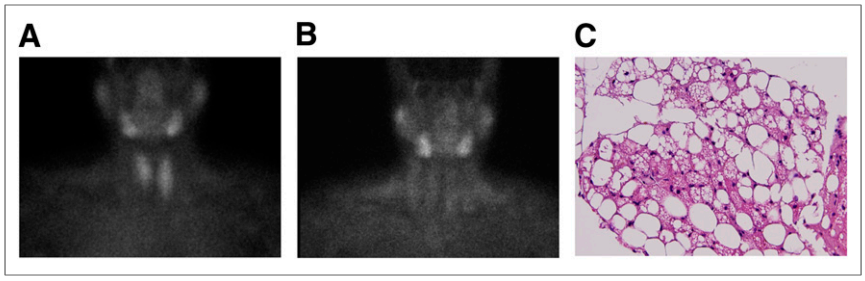

FIGURE 1. A 54-y-old woman with clinical hyperparathyroidism. (A and B) Coronal images of parathyroid adenomas using ^{99m}Tc-MIBI SPECT at 20 min (A) and 2 h (B) show increased uptake in neck and upper thorax, areas associated with human BAT. (C) Tissue was resected and studied using hematoxylin and eosin staining.

creased tracer retention in a mantlelike appearance in the regions of the neck and upper thorax, areas known to be enriched with human BAT typically (Figs. 1A and 1B). Biopsy of the tissue revealed brown adipocytes with typical multilocular lipid droplets and polygonal cells (Fig. 1C) (*8,31*). We next turned to SPECT/CT to provide a definitive correlation between adipose tissue identified as ^{99m}Tc-MIBI–avid and histologic proof of brown adipocytes. Every ^{99m}Tc-MIBI SPECT/CT scan done for the purpose of localizing parathyroid adenomas over a 22-mo interval was reviewed. Of the 74 patients (19 men and 49 women, 58 ± 15 y old [mean ± SD]), 4 (5.4%) demonstrated substantially increased uptake in the distinct fascial plane within the cervical and supraclavicular regions where BAT is located (Figs. 2A and 2B) (*7*). From a representative patient, biopsies from the subcutaneous WAT and ^{99m}Tc-MIBI–avid deeper neck adipose tissue were obtained. The microscopic and ultrastructural appearances were consistent with WAT and BAT, respectively (Figs. 2C and 2D). WAT from the subcutaneous depots was yellow, with large unilocular adipocytes and little cytoplasm. In contrast, the ^{99m}Tc-MIBI–localized fat was brown and multilocular with a high density of ovoid mitochondria.

Gene Expression Profile of ^{99m}Tc-MIBI–Avid Adipose Tissue

Quantitative reverse transcriptase polymerase chain reaction was used to examine the gene expression profile of the 2 different adipose tissue depots. Compared with subcutaneous WAT, ^{99m}Tc-MIBI–avid fat had 180 times greater tissue-specific *UCP1* expression levels ($P < 0.001$) (Fig. 3). Additionally, genes enriched in human BAT, such as *DIO2, PGC1α, CideA* (*8*), were increased, whereas WAT-associated *leptin* (*3,32*) had lower expression levels in the deeper fat.

Comparing Blood Flow and Glucose Uptake in Activated Rodent BAT

After determining that ^{99m}Tc-MIBI–avid adipose tissue is BAT in human tissue, we turned to the mouse model to define the physiologic changes resulting from pharmacologic stimulation of BAT. For each tracer, male 129SVE mice were administered either the β_3-adrenergic receptor agonist CL-316,243 (1 mg/kg) ($n = 16$) or saline control ($n = 16$). ^{18}F-FDG PET/CT ($n = 8$ for each of the 2 treatments) was used to reflect glucose uptake, and ^{99m}Tc-MIBI SPECT/CT ($n = 8$ for each of the 2 treatments) was given to measure tissue perfusion. CL-316,243 increased heart rate by 23% and respiratory rate by 85% ($P < 0.001$) (Supplemental Fig. 2). ^{18}F-FDG PET/CT imaging done 2 h after stimulation revealed significantly increased uptake in the interscapular BAT of CL-316,243 mice, compared with saline control mice (Figs. 4A and 4B). Uptake in the myocardium was also significantly elevated. To confirm the observed changes, we resected BAT, WAT, skeletal muscle, heart, and liver and quantified the %ID/g × kg (*21*). Even before stimulation, BAT retained more ^{18}F-FDG than did the other tissues and rose by 440% when stimulated by CL-316,243 ($P < 0.01$) (Fig. 4C). Other tissues showing CL-316,243–induced increases in ^{18}F-FDG were WAT, skeletal muscle, and heart. When the analogous study was done with ^{99m}Tc-MIBI, uptake in BAT was comparatively less than in liver and heart (Figs. 5A and 5B). The retained tracer in the resected tissues confirmed these findings, as %ID/g × kg in BAT increased by only 61% ($P < 0.01$), and there were no significant changes in WAT, skeletal muscle, liver, or heart (all $P > 0.05$) (Fig. 5C). Thus, specific pharmacologic stimulation of BAT led to a much greater increase in glucose uptake than tissue perfusion.

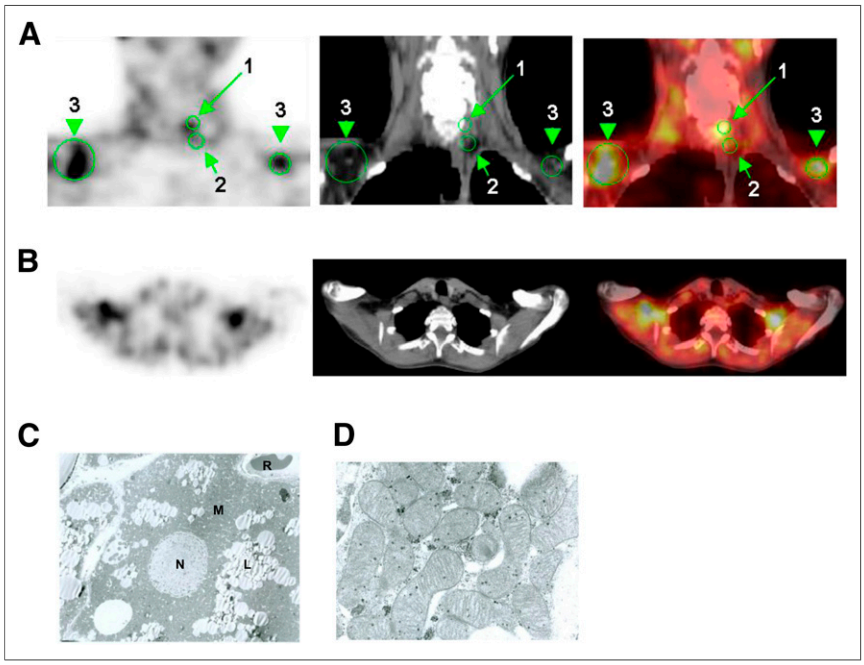

FIGURE 2. A 57-y-old woman with clinical hyperparathyroidism. (A and B) Coronal (A) and transaxial (B) slices of SPECT, CT, and fused SPECT/CT imaging of ^{99m}Tc-MIBI uptake show focal abnormal uptake posterior to mid pole of left thyroid lobe, compatible with reported parathyroid adenoma. Arrows indicate parathyroid adenoma (1), site of deep tissue biopsy (2), and main depot of BAT in supraclavicular space (3). (C and D) Osmium tetroxide staining of biopsied tissue shows individual brown adipocytes (C) and foci of ovoid mitochondria with dense cristae (D). L = lipid droplets; M = mitochondria; N = nucleus; R = red blood corpuscle.

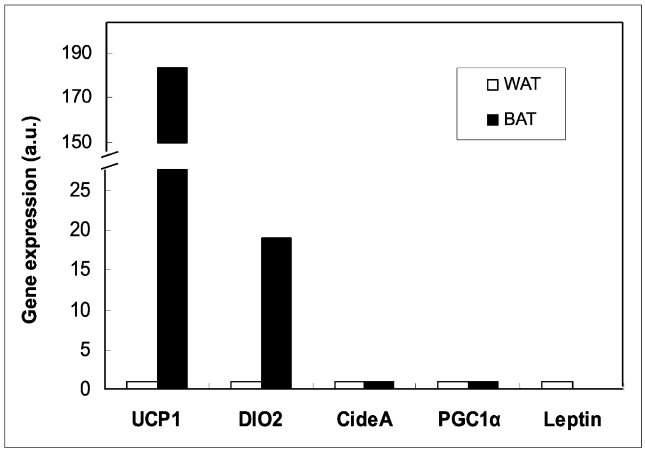

FIGURE 3. Quantitative reverse transcriptase polymerase chain reaction of subcutaneous WAT and site-directed biopsy of ^{99m}Tc-MIBI–avid tissue from single volunteer. Letpin is marker of WAT, and UCP1 is marker of BAT. Expression levels are in arbitrary units normalized to 36B4.

DISCUSSION

From the time that BAT was identified as a functional tissue in adult humans (*6–10*), there has been great interest in using BAT energy expenditure to treat obesity and metabolic dysregulation. When activated by mild cold exposure, adult human BAT has an energy expenditure of up to several hundred kilocalories per day (*18*). The broad reliance on ^{18}F-FDG PET/CT imaging has allowed the comparison of results among investigators, but the ability to describe other features of BAT physiology becomes more limited. Progress is being made in this area, with the introduction of new tracers such as ^{18}F-fluorobenzyl triphenyl phosphonium to measure thermogenesis (*33*) and the simultaneous use of combinations of ^{15}O-H_2O, ^{15}O-O_2, and ^{11}C-acetate along with ^{18}F-FDG to quantify blood flow, aerobic respiration, and glucose uptake (*11,17,18*). However, these and other radiotracers are either not yet approved for use in humans or are not readily available. ^{99m}Tc-MIBI meets these criteria and provides the opportunity to measure BAT mass and activity using SPECT/CT imaging. Prior studies have already indicated the possibility that ^{99m}Tc-MIBI could be used to detect BAT in adult humans (*23–26*). Here we have presented evidence strongly suggestive that ^{99m}Tc-MIBI localizes to human BAT and have demonstrated its utility in measuring BAT activity in response to pharmacologic activation.

Both the rate of detection of unstimulated BAT (5.4%) and the anatomic location seen using ^{99m}Tc-MIBI SPECT/CT imaging match the findings reported with ^{18}F-FDG PET/CT (*7,34*), indicating that both tracers are localizing to the same tissue. This pattern of tracer avidity is consistent with their molecular structures. The glucose analog ^{18}F-FDG localizes to tissues with high metabolic activity. ^{99m}Tc-MIBI is a lipophilic cation that is retained in tissues with high perfusion rates, particularly those enriched with mitochondria, which have a large negative transmembrane potential (*35*). The ultrastructural and gene expression findings presented here demonstrate how human brown adipocytes can be particularly avid for both ^{18}F-FDG and ^{99m}Tc-MIBI. These features also have direct clinical relevance since human neck BAT lies close to the parathyroid glands. Clinicians should be careful to ensure that increased ^{99m}Tc-MIBI uptake is from parathyroid tissue and not a false-positive signal from BAT.

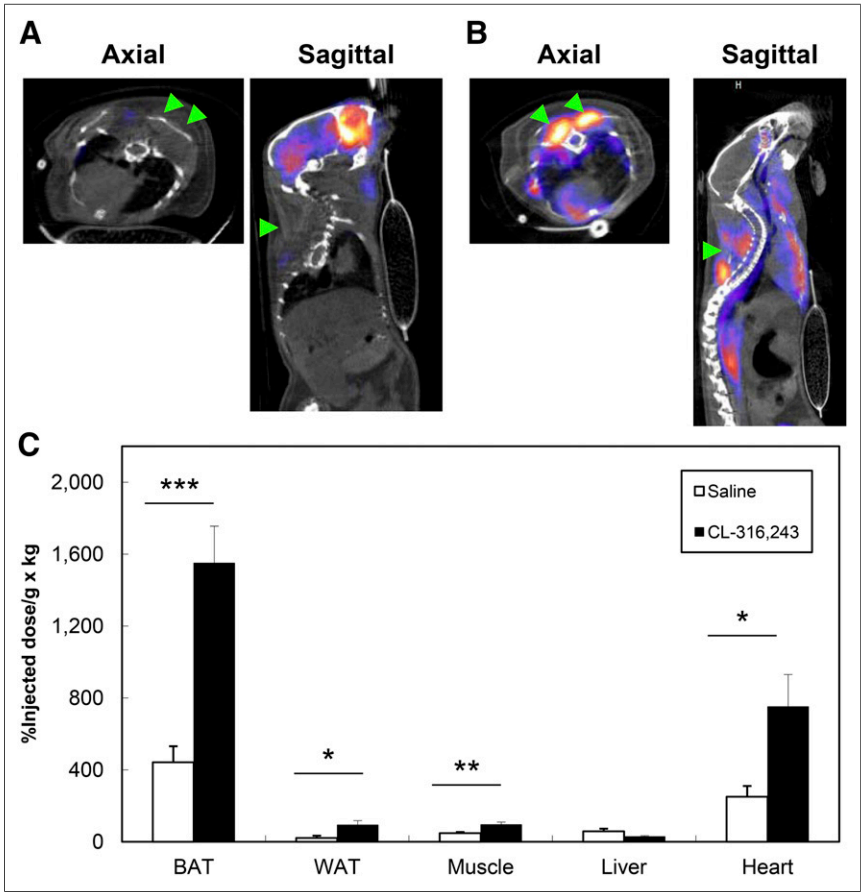

FIGURE 4. PET/CT axial and sagittal images of 129SVE mice demonstrating uptake in interscapular BAT (arrows) 120 min after injection of ^{18}F-FDG. (A and B) Mice were given either saline control (A) or CL-316,243 (1 mg/kg) (B). (C) After imaging, tissues were resected, and activity was quantified as %ID/g × kg. *$P < 0.05$. **$P < 0.01$. ***$P < 0.001$.

Because BAT is an organ designed to generate heat at a rate of up to 300 W/kg (*3*), a high rate of BAT perfusion is necessary to provide oxygen and fuel and to transfer the heat before thermal injury occurs. When studied in response to cold exposure, BAT tissue perfusion increases, but less so than glucose uptake (*11*). The significant correlation between these 2 independent measures of metabolism justifies the wide use of ^{18}F-FDG to measure relative changes in BAT activity. However, it remains unclear what the fate of the glucose is. The fact that glucose utilization exceeds that of blood flow indicates that activated BAT likely uses glucose for several metabolic purposes. Internal lipid stores are the primary fuel for BAT and are used rapidly in response to cold exposure (*3,36*). The glucose may be used for

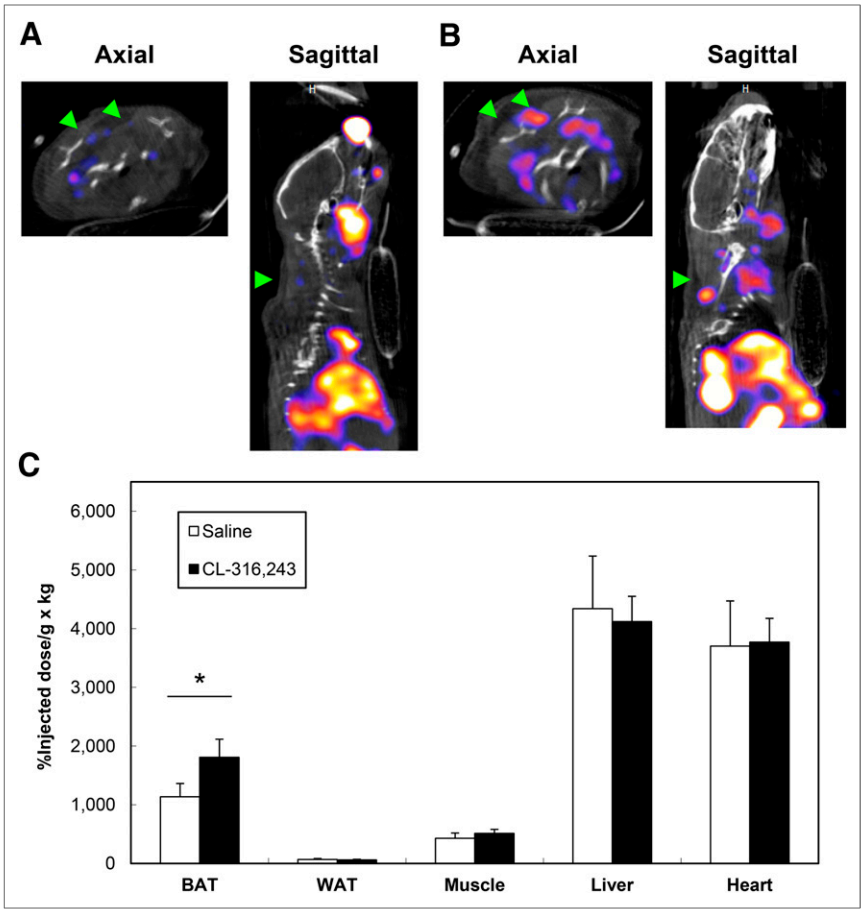

FIGURE 5. SPECT/CT axial and sagittal images of 129SVE mice demonstrating uptake in interscapular BAT (arrows) 120 min after injection of ^{99m}Tc-MIBI. (A and B) Mice were given either saline control (A) or CL-316,243 (1 mg/kg) (B). (C) After imaging, tissues were resected, and activity was quantified as %ID/g × kg. *$P < 0.05$.

lipogenesis, glycolysis, anaplerosis, and uncoupled aerobic respiration (*37*). The simultaneous activity of these multiple pathways could explain the relatively higher rate of glucose utilization seen during BAT activation. Additional studies are required to determine how glucose is used in quiescent and activated BAT and how the measured uptake with ^{18}F-FDG correlates with these different processes.

A limitation of this study is that we did not prospectively administer ^{99m}Tc-MIBI to humans to show changes in tracer uptake in response to BAT stimulation. Rather, we relied on the site-directed biopsies to support the presence of human BAT and used the rodent studies to show the dynamic changes in BAT function. In addition, we did not simultaneously evaluate the changes in uptake of ^{99m}Tc-MIBI and ^{18}F-FDG. In the mice, to permit detection of both tracers, this approach would have required doing the studies sequentially and not being able to accurately measure each tracer's uptake on biopsy. However, the degree of BAT stimulation was likely to be similar with both tracers as evidenced by the nonsignificant difference between the heart and respiratory rates seen after treatment with CL-316,243 and vehicle. Another issue is that uptake of ^{99m}Tc-MIBI is driven not only by perfusion but also by the expression of p-glycoprotein (*38*), levels of which are unknown in BAT. Future studies should examine the expression of p-glycoprotein in rodent and human BAT. Furthermore, stimulation of BAT leads to mitochondrial uncoupling and a lowering of the transmembrane potential, which could reduce ^{99m}Tc-MIBI uptake. An alternative measure to quantify blood flow is contrast ultrasound, which has been used in rodent BAT (*39*) and could be correlated with ^{99m}Tc-MIBI uptake. Nevertheless, our findings are qualitatively similar to what has been reported with other markers of blood flow after cold-mediated activation of BAT in humans (*11*) and rodents (*21*).

CONCLUSION

We demonstrate that the accessible tracer ^{99m}Tc-MIBI may be used to detect BAT via SPECT/CT in humans and can provide information about changes in its blood flow. Understanding the physiologic function and clinical utility of BAT energy expenditure will likely require multiple complementary tracers.

DISCLOSURE

The costs of publication of this article were defrayed in part by the payment of page charges. Therefore, and solely to indicate this fact, this article is hereby marked "advertisement" in accordance with 18 USC section 1734. This work was supported by NIH grants DK087317, DK081604, DK046200, DK077097, RR025757, and P30 DK036836 from the National Institute of Diabetes and Digestive and Kidney Diseases (NIDDK), the Clinical Translational Science Award UL1RR025758 to Harvard University and BIDMC from the National Center for Research Resources, Harvard Catalyst. The Harvard Clinical and Translational Science Center (NIH award UL1 RR 025758 and financial contributions from Harvard University and its affiliated academic health care centers), the Clinical Investigator Training Program (Beth Israel Deaconess Medical Center–Harvard/MIT Health Sciences and Technology, in collaboration with Pfizer and Merck), and the Eli Lilly Foundation. No other potential conflict of interest relevant to this article was reported.

ACKNOWLEDGMENTS

We thank Elaine Lunsford and Kyle Robichaud for their excellent technical support at the Longwood Small Animal Imaging Facility, Michael Rourk and Graham Smythe for their expertise in maintaining the animal colonies, Hillary Keenan for her biostatistical advice, Chris Cahill at the Joslin Diabetes Center Microscopy Core for his histologic work, the teams of OR nurses for their assistance in tissue collection, J. Anthony Parker for his thoughts on the physiologic role of ^{99m}Tc-MIBI, and C. Ronald Kahn for his input in preparing the manuscript. Finally, we are grateful to our volunteers for their commitment to the studies.

REFERENCES

1. Haslam DW, James WP. Obesity. *Lancet.* 2005;366:1197–1209.
2. Cypess AM, Kahn CR. Brown fat as a therapy for obesity and diabetes. *Curr Opin Endocrinol Diabetes Obes.* 2010;17:143–149.
3. Cannon B, Nedergaard J. Brown adipose tissue: function and physiological significance. *Physiol Rev.* 2004;84:277–359.
4. Hany TF, Gharehpapagh E, Kamel EM, Buck A, Himms-Hagen J, von Schulthess GK. Brown adipose tissue: a factor to consider in symmetrical tracer uptake in the neck and upper chest region. *Eur J Nucl Med Mol Imaging.* 2002;29:1393–1398.
5. Cohade C, Osman M, Pannu HK, Wahl RL. Uptake in supraclavicular area fat ("USA-Fat"): description on ^{18}F-FDG PET/CT. *J Nucl Med.* 2003;44:170–176.
6. van Marken Lichtenbelt WD, Vanhommerig JW, Smulders NM, et al. Cold-activated brown adipose tissue in healthy men. *N Engl J Med.* 2009;360:1500–1508.
7. Cypess AM, Lehman S, Williams G, et al. Identification and importance of brown adipose tissue in adult humans. *N Engl J Med.* 2009;360:1509–1517.
8. Virtanen KA, Lidell ME, Orava J, et al. Functional brown adipose tissue in healthy adults. *N Engl J Med.* 2009;360:1518–1525.
9. Zingaretti MC, Crosta F, Vitali A, et al. The presence of UCP1 demonstrates that metabolically active adipose tissue in the neck of adult humans truly represents brown adipose tissue. *FASEB J.* 2009;23:3113–3120.
10. Saito M, Okamatsu-Ogura Y, Matsushita M, et al. High incidence of metabolically active brown adipose tissue in healthy adult humans: effects of cold exposure and adiposity. *Diabetes.* 2009;58:1526–1531.
11. Orava J, Nuutila P, Lidell ME, et al. Different metabolic responses of human brown adipose tissue to activation by cold and insulin. *Cell Metab.* 2011;14:272–279.
12. Pfannenberg C, Werner MK, Ripkens S, et al. Impact of age on the relationships of brown adipose tissue with sex and adiposity in humans. *Diabetes.* 2010;59:1789–1793.
13. Bredella MA, Fazeli PK, Freedman LM, et al. Young women with cold-activated brown adipose tissue have higher bone mineral density and lower pref-1 than women without brown adipose tissue: a study in women with anorexia nervosa, women recovered from anorexia nervosa, and normal-weight women. *J Clin Endocrinol Metab.* 2012;97:E584–E590.
14. Cypess AM, Chen YC, Sze C, et al. Cold but not sympathomimetics activates human brown adipose tissue in vivo. *Proc Natl Acad Sci USA.* 2012;109:10001–10005.
15. Vosselman MJ, van der Lans AA, Brans B, et al. Systemic beta-adrenergic stimulation of thermogenesis is not accompanied by brown adipose tissue activity in humans. *Diabetes.* 2012;61:3106–3113.
16. Vrieze A, Schopman JE, Admiraal WM, et al. Fasting and postprandial activity of brown adipose tissue in healthy men. *J Nucl Med.* 2012;53:1407–1410.
17. Muzik O, Mangner TJ, Granneman JG. Assessment of oxidative metabolism in brown fat using PET imaging. *Front Endocrinol (Lausanne).* 2012;3:15.
18. Ouellet V, Labbe SM, Blondin DP, et al. Brown adipose tissue oxidative metabolism contributes to energy expenditure during acute cold exposure in humans. *J Clin Invest.* 2012;122:545–552.
19. Wackers FJ, Berman DS, Maddahi J, et al. Technetium-99m hexakis 2-methoxyisobutyl isonitrile: human biodistribution, dosimetry, safety, and preliminary comparison to thallium-201 for myocardial perfusion imaging. *J Nucl Med.* 1989;30:301–311.
20. Marshall RC, Leidholdt EM Jr., Zhang DY, Barnett CA. Technetium-99m hexakis 2-methoxy-2-isobutyl isonitrile and thallium-201 extraction, washout, and retention at varying coronary flow rates in rabbit heart. *Circulation.* 1990;82:998–1007.
21. Baba S, Engles JM, Huso DL, Ishimori T, Wahl RL. Comparison of uptake of multiple clinical radiotracers into brown adipose tissue under cold-stimulated and nonstimulated conditions. *J Nucl Med.* 2007;48:1715–1723.
22. Morrison SF. 2010 Carl Ludwig Distinguished Lectureship of the APS Neural Control and Autonomic Regulation Section: central neural pathways for thermoregulatory cold defense. *J Appl Physiol.* 2011;110:1137–1149.
23. Higuchi T, Kinuya S, Taki J, et al. Brown adipose tissue: evaluation with ^{201}Tl and ^{99m}Tc-sestamibi dual-tracer SPECT. *Ann Nucl Med.* 2004;18:547–549.
24. Kyparos D, Arsos G, Georga S, et al. Assessment of brown adipose tissue activity in rats by ^{99m}Tc-sestamibi uptake. *Physiol Res.* 2006;55:653–659.
25. Belhocine T, Shastry A, Driedger A, Urbain JL. Detection of ^{99m}Tc-sestamibi uptake in brown adipose tissue with SPECT-CT. *Eur J Nucl Med Mol Imaging.* 2007;34:149.
26. Goetze S, Lavely WC, Ziessman HA, Wahl RL. Visualization of brown adipose tissue with ^{99m}Tc-methoxyisobutylisonitrile on SPECT/CT. *J Nucl Med.* 2008;49:752–756.
27. Chen YI, Cypess AM, Sass CA, et al. Anatomical and functional assessment of brown adipose tissue by magnetic resonance imaging. *Obesity (Silver Spring).* 2012;20:1519–1526.
28. Akram K, Parker JA, Donohoe K, Kolodny G. Role of single photon emission computed tomography/computed tomography in localization of ectopic parathyroid adenoma: a pictorial case series and review of the current literature. *Clin Nucl Med.* 2009;34:500–502.
29. Cypess AM, White AP, Vernochet C, et al. Anatomical localization, gene expression profiling and functional characterization of adult human neck brown fat. *Nat Med.* 2013;19:635–639.
30. Torriani M, Fitch K, Stavrou E, et al. Deiodinase 2 expression is increased in dorsocervical fat of patients with HIV-associated lipohypertrophy syndrome. *J Clin Endocrinol Metab.* 2012;97:E602–E607.
31. Cinti S. The adipose organ. *Prostaglandins Leukot Essent Fatty Acids.* 2005;73:9–15.
32. Timmons JA, Wennmalm K, Larsson O, et al. Myogenic gene expression signature establishes that brown and white adipocytes originate from distinct cell lineages. *Proc Natl Acad Sci USA.* 2007;104:4401–4406.
33. Madar I, Isoda T, Finley P, Angle J, Wahl R. ^{18}F-fluorobenzyl triphenyl phosphonium: a noninvasive sensor of brown adipose tissue thermogenesis. *J Nucl Med.* 2011;52:808–814.
34. Cohade C, Mourtzikos KA, Wahl RL. "USA-Fat": prevalence is related to ambient outdoor temperature—evaluation with ^{18}F-FDG PET/CT. *J Nucl Med.* 2003;44:1267–1270.
35. Chiu ML, Kronauge JF, Piwnica-Worms D. Effect of mitochondrial and plasma membrane potentials on accumulation of hexakis (2-methoxyisobutylisonitrile) technetium(I) in cultured mouse fibroblasts. *J Nucl Med.* 1990;31:1646–1653.
36. Baba S, Jacene HA, Engles JM, Honda H, Wahl RL. CT Hounsfield units of brown adipose tissue increase with activation: preclinical and clinical studies. *J Nucl Med.* 2010;51:246–250.
37. Hue L, Taegtmeyer H. The Randle cycle revisited: a new head for an old hat. *Am J Physiol Endocrinol Metab.* 2009;297:E578–E591.
38. Sun SS, Shiau YC, Lin CC, Kao A, Lee CC. Correlation between P-glycoprotein (P-gp) expression in parathyroid and Tc-99m MIBI parathyroid image findings. *Nucl Med Biol.* 2001;28:929–933.
39. Baron DM, Clerte M, Brouckaert P, et al. In vivo noninvasive characterization of brown adipose tissue blood flow by contrast ultrasound in mice. *Circ Cardiovasc Imaging.* 2012;5:652–659.